Case Studies in Thermal Engineering 74 (2025) 106746

Contents lists available at ScienceDirect

Case Studies in Thermal Engineering

journal homepage: www.elsevier.com/locate/csite

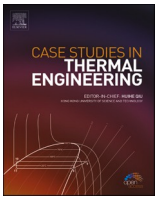

Ocean thermal energy conversion systems: The heat losses effect of the cold-water pipe

Lazaros Aresti [a,b], Toula Onoufriou [a,b], Constantine Michailides [c], Paul Christodoulides [a,b,*]

[a] EMERGE Centre of Excellence, Lemesos, Cyprus
[b] Faculty of Engineering and Technology, Cyprus University of Technology, Lemesos, Cyprus
[c] Department of Civil Engineering, International Hellenic University, Serres University Campus, Greece

ARTICLE INFO

Keywords:
Ocean thermal energy conversion
OTEC
Heat transfer
OTEC cold water pipe

ABSTRACT

Ocean Thermal Energy Conversion (OTEC) systems are categorized as Renewable Energy Systems (RES), as the natural sea temperature difference (ΔT), between the surface water and the deep seawater, can be exploited either to produce electricity or to deliver a by-product. The sea water temperature varies according to location/country, also depending on sea depth and distance from shore. Therefore, the minimum distance from shore can vary in order to meet the required ΔT for the system to perform in a beneficial manner. The present study investigates the effect of such cases, by examining the magnitude of the heat transfer loss of the cold-water pipes (CWPs), in terms of the outcome in the theoretical efficiency of the system. CWPs are computationally investigated using the COMSOL Multiphysics software, to assess a more accurate ΔT. Contrary to this study, in most literature cases the ΔT used in the performance estimations, is the one found on location and without any computational process. The CWP pump was also assessed in terms of required power and case. A parametric analysis of the size of the CWP, mass flowrate, pumping power, pipe material, distance from shore, and a comparison between onshore and offshore positioning of the OTEC systems is presented. Offshore systems seem to exhibit a desired lower temperature difference by up to 86 % from that of long-CWP onshore systems. Overall results indicate, even considering the non-ideal case of heat loss, OTEC systems - onshore or offshore - may become viable, but site specific ΔT estimations are required per case.

1. Introduction

The energy acquired (or transformed) from natural sources that can be revived on a rate higher than can be exploded, finds applications through Renewable Energy Systems (RES). In the case of oceans/seas and possible marine applications, one may refer to solar energy absorbed by the oceans/seas in the form of heat energy. Thereby, the natural sea temperature difference (ΔT), between the surface water and the deep seawater, can be exploited either to produce electricity or to deliver a by-product through the RES called Ocean Thermal Energy Conversion (OTEC) systems. The OTEC concept is not recent and was conceptualized by Jacques-Arsène D'Arsonval in 1881, while later – in the 1920s – Georges Claude constructed the first experiment in Cuba [1,2].

Given the temperature difference between the deep seawater and surface seawater, thermodynamic cycles, such as Rankine cycle,

* Corresponding author. EMERGE Centre of Excellence, Lemesos, Cyprus.
E-mail address: paul.christodoulides@cut.ac.cy (P. Christodoulides).

https://doi.org/10.1016/j.csite.2025.106746
Received 28 January 2025; Received in revised form 12 June 2025; Accepted 23 July 2025
Available online 24 July 2025
2214-157X/© 2025 The Authors. Published by Elsevier Ltd. This is an open access article under the CC BY license (http://creativecommons.org/licenses/by/4.0/).

can be used to generate electricity with the use of a turbine [3–8]. There are different cycles and configurations that could be used, different working fluids [9], as well as more novel approaches like the temperature lift cycle [10]. The seawater temperature however varies with location (for instance, depending on the distance from the equator) and therefore, one of the major disadvantages of the OTEC technology, is the lack of high-enough ΔT availability values in every geographic location/country. It should be mentioned here that the net power output of an OTEC system could decrease by up to 10 % with every temperature difference drop of 1 °C [11]. The tropic regions and the equatorial region in general have an advantage over other locations, with high surface seawater temperatures and less variations throughout the year. OTEC systems are not only highly dependent on high-enough ΔT, but also on the location on where this difference can be found. For example, when the required ΔT is satisfied at a 1 km depth and a short distance from the shore, an onshore system could be more realistic; otherwise an offshore system should be adopted. The distance from shore in this case describes the length of a straight line between the location of the deep cold seawater and the potential onshore location of the system, where the pipe will have to transfer the cold water. The OTEC system therefore requires two intake pipes, one that draws the deep cold seawater and is placed at the seabed, and another one that draws the surface warm seawater.

As is the case with geothermal energy and hydroelectric energy, OTEC can have the advantage of continuous operation [12]. In addition to electricity production, OTEC systems (depending on the cycle) can provide water desalination, hydrogen production, aquaculture and air-conditioning [13]. OTEC systems have seen considerable attention at the end of the twentieth century [14–18], but have not seen a major advancement since, due to the availability of more easily applicable RES (such as solar). Recently however, the interest in OTEC systems has been revived due to the energy crisis and the race for green energy production and CO2 emissions reduction [19,20].

Several OTEC case studies, onshore or offshore (real, pilot or theoretical), exist in the literature [21–30]. Several indicative examples are presented here. For example, a proposed theoretical designed OTEC plant of 5 MW net power using an offshore structure was studied on the assumption of a steady 4.5 °C cold seawater temperature with a constant flow at 13.9 $m^3 s^{-1}$ and a pump efficiency of 72 % [31]. Due to the choice of a large inner diameter (2.72m), the cold-water pipe (CWP) material was chosen to be glass fibre reinforced plastic (FRP). Being an offshore system the CWP was 1 km long. In another study, the potential of an OTEC plant, of higher power, 100 MW gross/100 MW net power, was examined for a relatively high mass flowrate of 366000 kg s^{-1} (366 $m^3 s^{-1}$) in the state of Florida, USA [32]. For this particular case, the ideal depth of 1 km, and the estimated highest temperature difference, is located far from the Florida shore (at approximately 98 km). A lower temperature difference of approximately 18 °C is possible at a significantly shorter distance from shore, at 12 km. Based on the above, an offshore structure with 1 km CWP length, a pipe diameter of 10m and with CWP pump efficiency assumed at 80 %, was proposed in order for maximum power output. In a more recent study a 10 MW OTEC system in Morotai Island, North Maluku, Indonesia was proposed for a mass flowrate of 29000 kg s^{-1} (29 $m^3 s^{-1}$) [33]. Following the assumptions in Refs. [34,35], the same temperature for the CWP at the inlet of the pipe and at the inlet of the condenser was assumed. Regarding the determination of potential locations of high thermal gradient (i.e., high enough ΔT) for OTEC application can be found in Ref. [36], where for $\Delta T \geq 20$ °C and a distance from shore ≤10 km, a list of locations was presented. The average distance from shore was at 7.7 km, with the minimum length at 2.3 km and the maximum at 10.9 km. It must be emphasized here, that for the sake of simplicity, in OTEC modelling studies, no heat losses between the CWP inlet and the condenser inlet are considered, with the temperatures assumed to be equal [37–39]. Numerical modelling of OTEC plants has also progressed from simple cycle calculations to high-fidelity CFD platforms that optimise flow fields and component geometry in tandem. Liu et al. outline this evolution and highlight how integrated optimization is displacing earlier lumped-parameter approaches [40]. Wang and co-workers, for example, linked zeotropic-mixture selection with turbine sizing and reported several-point gains in first-law efficiency [41].

Despite these advances, almost all of the cited studies impose fixed warm- and cold-seawater boundary temperatures, even though Rajagopalan & Nihous [42] and Giostri et al. [43] separately estimate that a 1 °C shift at either intake can alter net power output by roughly 15 %. Closing this gap requires careful analysis of the CWP, which frequently has a large length and might gain several degrees °C during ascent. Petroleum and geothermal research offer immediately applicable tools with capturing the convection–conduction effects that remain relevant. For example, Zhou et al. [44] compared analytical solutions with a numerical solution (using COMSOL Multiphysics) for ground heat exchangers in the presence of groundwater flow under convective boundary conditions. The authors have noted that at low seepage velocities, additional vertical flow cools the pipe wall noticeably, however once the horizontal seepage velocities is high, any extra vertical circulation makes a negligible difference to temperature. At the component scale, Saeidi et al. [45] numerically investigated a shallow spiral ground heat exchanger, with fitted fins, with the 1D-3D approach applied in COMSOL. The specific approach was also verified and validated. A ground heat-exchanger shell was modelled by Meikandan et al. [46], where the model was verified and validated using a 3D approach and experimental data.

In most cases for OTEC performance estimation found in the literature and commented in this study, the condenser and evaporator inlet temperatures are respectively the temperatures of the deep seawater and the surface seawater on location, not considering any losses between the pipes and the surrounding environment. Any potential temperature losses/gains to the environments are directly connected to the performance of the system, as the OTEC systems are heavily reliant on a very small temperature difference to run a heat engine.

The actual goal intended here is to computationally investigate the effect of the CWP size (diameter and length) on heat losses and their *magnitude*, and consequently on temperature difference, pumping power and efficiency of OTEC systems. Doing this, can answer the feasibility question of applying/using OTEC systems at all (constituting a novelty as – to our knowledge – no other such study exists for OTECs). The methodology is described in Section 2, with a parametric analysis of the size of the CWP, mass flowrate, pumping power, pipe material, distance from shore, and a comparison between onshore and offshore positioning of the OTEC systems performed in Section 3. The study is concluded in Section 4.

2. Materials and methods

For the estimation of the performance of the OTEC systems, seawater temperature difference, from the seabed (of approximately 1 km) to the sea surface, is assumed by most researchers to be approximately 20–24 °C based on the available location data [47–50]. With such temperature difference (ΔT = 20 °C) the OTEC system Carnot efficiency is estimated at 6.7 % (see also Fig. 3). There are though cases of hybrid cycles yielding higher system performance [51]. In regions than can maintain a ΔT of 17–18 °C or higher, the OTEC systems can maintain a yearly maximum efficiency [52]. However, with the heat losses that occurs at the CWP, the actual ΔT that applies for the thermodynamic cycle's estimations might differ from the assumed ΔT. The study performed here is generic for any OTEC system, focusing on the effect of CWP on heat losses. However, data related to the location of an existing OTEC system installed in Hawaii (at the Natural Energy Laboratory, Kailua-Kona, HI, USA) is considered here, as presented in Table 1 and Fig. 1. Note that the selected location (presented in Table 1 and Fig. 1) is at an approximately 10 km distance from shore.

The CWP is placed in deep seawater and it is essential to be located at the lowest possible water temperature. The available size of the CWP, namely the diameter and the length of the pipe, has a direct effect on the pumping power and the pressure losses (see equations described below). Clearly, the length of the pipe has a major impact in terms of investment and capital cost of the system, due to the added cost for the material and the labour. The CWP has to not only pump the required seawater but also to withstand high mechanical loads. It has been described in the literature [53,54] that the mechanical loads can be due to the suction stress, waves and currents' loads, and pipe weight stress. The materials that are used for such piping systems are high density polyethylene (HDPE) or fibre reinforced plastic (FRP). Large diameter HDPE pipes placed in the sea (offshore) find applications for intake cooling seawater in large scale power plants [55]. HDPE high resistance to corrosion could make it also a favourable solution for the sea environment. Previous projects [56,57], such as the OTEC project by Lockhead Martin at Kumejima Island, used HDPE pipes reinforced with steel; it was noted that due to the diameter limitation of the HDPE pipes (maximum 2.5m), this solution is mostly suitable for plants with a capacity of 2.5 MW or lower. FRP is recommended for larger diameter pipes and larger capacity plants [58]. In the present study, HDPE pipes are selected as CWP for the lower capacity systems, while FRP material is selected for the higher capacity system; their specification can be seen in Table 2.

To meet the aim of the current study as described in the Introduction, data from previous case studies are used for the computational investigation of how the CWP size (diameter and length) affects the pumping power and the efficiency of OTEC systems, also suggesting the most advantageous position (onshore versus offshore). Depending on the capacity of the OTEC system, the CWP size and the flowrate vary to satisfy the required load. In Refs. [59,60] the CWP was assumed to have a flowrate of 2–4 $m^3\ s^{-1}$ corresponding to every net MW of electricity required. With this assumption, and with the density of the seawater estimated at 1023.6 kg m^{-3} (at a temperature of 25 °C and salinity of 35 g kg^{-1}), the mass flowrate will be approximately 2047–4094 kg s^{-1} (~2–4 $m^3 s^{-1}$) for every MW electricity required. These values are in line with the estimated flowrates in more recent studies, where similar flowrates are observed [54,61], including demonstration plants (such as the demonstration plant in Kiribati, Pacific Islands Region) [62]. Table 2 shows the required data used for the computational investigation for different capacities, namely 10 MW, 2.3 MW, 1 MW and 20 kW, based on case studies gathered from the literature.

The required pipe length (horizontal distance) also depends on the morphology of the seabed and the distance (from shore) to reach the desirable 1 km sea depth or the suitable sea temperature (lowest possible ~ 4–6 °C). Such example is the KRISO project where the required depth of 3.5–4 km for the specific project is within a 5 km horizontal distance from shore [62,65]. The geometry of the CWP is taken in a realistic scenario approach and a simplistic approach where the pipe is being placed linearly towards the seabed (seen in Fig. 2). The pipe characteristics selected for the computational investigation in this research are presented in Table 2.

The simulations can follow a similar methodology to that applied in geothermal energy, where the heat transfer influence in shallow geothermal energy systems is between the ground heat exchangers and the ground [66–68]. Similarly, the surrounding environment for the CWP in OTEC systems is the seawater and the seabed. The basic equation governing the convective and conductive heat transfer in the system under investigation is:

$$\rho c_p \frac{\partial T}{\partial t} + \rho c_p u \cdot \nabla T + \nabla q = Q \tag{1}$$

where t denotes time [s], ρ denotes the density [kg m^{-3}], u the velocity [m s^{-1}], T the temperature [K], c_p the specific heat capacity [J kg^{-1} K^{-1}], Q the power density of the heat source [W m^{-3}], and heat flux q [W m^{-2}] deriving from the Fourier's law of heat conduction.

Table 1
Seawater Temperature data with coordinates referring to the islands of Hawaii.

Title	Seawater Temperature Data
Description	Sea water temperature potential at different depths
Credits	EU Copernicus Marine Service information
Publisher	https://marine.copernicus.eu
Dataset	global-analysis-forecast-phy-001-024-monthly
Variable	sea water potential temperature [°C]
Geometry	POINT(-156.1589169303501 19.72676261793143)
Depth Levels	from sea surface to 1000 m

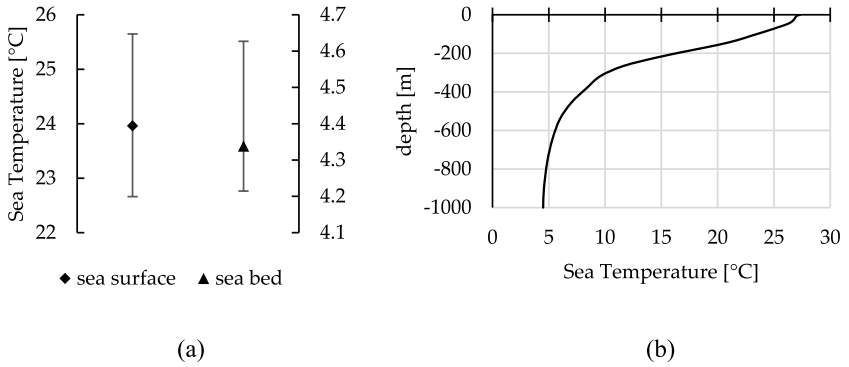

Fig. 1. Temperature values based on data from Table 1 with (a) Average sea temperature with yearly maximum and minimum values for the sea surface (20m) and sea bed (1000m), and (b) sea temperature depth profile.

Table 2
Parameters used in the current study simulations.

Capacity	20 kW	1 MW [62]	2.3 MW [63]	10 MW [58]
Material	HDPE			FRP
CWP inner diameter [m]	0.7608	1.9022	2.3776	4.000
CWP outer diameter [m]	0.800	2.000	2.500	4.210
Thickness [m]	0.0392	0.0978	0.1224	0.21
CWP mass flowrate [kg s^{-1}]	0.045	1.805	8.500	20.400
Thermal conductivity [W m^{-1} K^{-1}]	0.51			0.58 [64]
CWP distance from shore [m]	(1)1000 (for vertical distance, e.g., floating structure), (2)3000, (3) 5000, (4) 7000, (5) 10000			

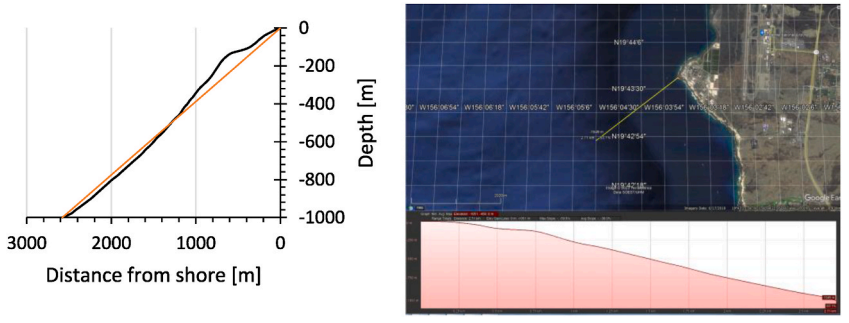

Fig. 2. Left: CWP realistic geometry (black) and simplified geometry (orange), and right: location taken from Google Earth Inc.

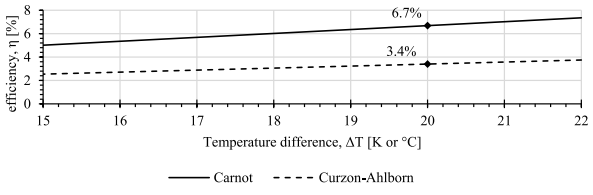

Fig. 3. Carnot efficiency and Curzon-Ahlborn with respect to temperature difference, for a steady surface seawater temperature of 26 °C (299.15K).

The COMSOL Multiphysics v6.1 software, with educational license, was selected to solve the convection-diffusion equation using a transient time-dependent analysis. This choice was primarily driven by the accessibility and availability of the software. Additionally, COMSOL offers a user-friendly interface and robust capabilities for solving both ordinary and partial differential equations (ODEs and PDEs) using the Finite Element Method (FEM), making it particularly well-suited for this type of numerical analysis. Another approach would be to solve the governing equations on a programming language such as MATLAB, however compared to MATLAB, which also offers PDE-solving capabilities, COMSOL provides a more intuitive graphical interface and built-in tools specifically optimized for

FEM-based Multiphysics simulations. The model was implemented using the 'Heat Transfer in Pipes' interface with the "novel" 1D approach. The elements count was changed for each case study as to satisfy a maximum element size of 30m, and a growth rate of 1.1.

Having a very large domain and a small pipe diameter (high scale difference), and using a 1:1 scale in a 2D or 3D environment, there is a need of high computational time and memory for generating the mesh (with equilateral cells) and providing a converged solution. This weakness could be overcome either by applying a scale to one of the directions [68], or with the use of 1D simplified version equation [69] on the pipes as shown below:

$$\rho A c_p \frac{\partial T}{\partial t} + \rho A c_p u e_t \cdot \nabla_t T = \nabla_t \cdot (A\lambda \nabla_t T) + \frac{1}{2} f_D \frac{\rho A}{d_i} |u| u^2 + Q_{wall} \tag{2}$$

where A is the area of the pipe [m^2], ue_t is the tangential velocity [m s^{-1}], λ the thermal conductivity [W m^{-1} K^{-1}], f_D the Darcy's friction factor based on Colebrook friction model, and d_i is the inner diameter of the pipe [m]. Q_{wall} is the heat conduction given by

$$Q_{wall} = \left(h_p Z\right)_{eff} (T_{ext} - T_{seawater}) \tag{3}$$

where T_{ext} is the external temperature at the pipe wall [K], $T_{seawater}$ the seawater temperature [K], $\left(h_p Z\right)_{eff}$ the effective value of the heat transfer coefficient of the pipe for a circular cross section $\left(h_p\right)$ [W m^{-2} K^{-1}], and Z the wall perimeter of the pipe [m]. Note that the boundary between the fluid and the tubes has an internal convective heat flux, with the convective heat transfer coefficient h_{int} depending on the Nusselt number Nu, which can be estimated with the internal film heat transfer model as

$$h_{int} = \mathrm{Nu} \frac{k}{D_{CWP,i}}, \mathrm{Nu} = 3.66 \tag{4}$$

where k is the heat transfer rate, and $D_{CWP,i}$ the inner diameter of the CWP. For further simplification, the model consists of only one domain, the CWP in a 2D environment. The material used for the fluid in the CWP is seawater with its properties changing according to the temperature and pressure. Of note is that the thermal conductivity can be affected by the salinity of the water, with a higher content of salinity having a lower thermal conductivity [70], compared to pure water.

Seawater density in terms of salinity and pressure can be estimated using the Thermodynamic Equation of Seawater 2010 (TEOS-10) formula [71–74]. The density, pressure and temperature at the seabed and the surface of the sea are considered constant and are based on the Marine Copernicus data (see Table 1). TEOS-10 was used to pre-estimate the density ρ as a function of Absolute Salinity s_a (obtained from Practical Salinity, s_p, via $s_a \approx 1.004715\, s_p$), temperature, and pressure P [dbar]. For all calculations the gibbs-seawater (gsw) toolbox [75] was used, which reproduces the Gibbs free-energy formulation of TEOS-10, $gsw_\rho(s_a,T,P)$, subsequently employed as an interpolation function in the COMSOL model so that it will be thermodynamically consistent with modern oceanographic data sets and climate-model outputs. Another approach (not applied here) would be to first estimate the bulk modulus at atmospheric pressure ($P = 0$), $K(s,T)$, followed by the Pressure corrections, $K(s,T,P)$, and to finally obtain the in-situ density at the desired pressure, $\rho(s,T,P)$.

Transient runs used the backward-differentiation (BDF) time-stepping scheme (order 1–5), with an adaptive time step starting at 60 s; relative solver tolerance was 10^{-3}. For each case the solution time was $<$ 1min with an 8-core Intel Xeon CPU and 16 GB RAM desktop PC.

It must be emphasized here that validation of the presented model is beyond the scope of the current research. This is due to the nature and the low maturity of the research done (especially academic) on OTEC systems, resulting in a lack of experimental data in the literature; the latter are actually confidential as the experiments and case studies performed involve enterprises. Hence, validation is left for a future research once real experimental data become available.

Instead, a *verification* of the computational model can be made through cases in the literature related to OTEC and equivalent geothermal energy systems [66,68,76,77]. The ground heat exchangers are essentially pipes exchanging heat with the ground by circulating water or an anti-freeze mixture solution fluid. This principle is therefore the equivalent as the OTEC pipes, with the difference that the OTEC pipes are submerged into the sea. In this case the exchange medium is considered to be the seawater, and the external temperature T_{ext} is considered to be constant. The sea temperature change with respect to the depth (y-axis), used as the external temperature of the pipe, is reported in the literature. The pipe external temperature T_{ext} is assumed to be constant since there is a constant movement (sea currents) of the sea. Although an OTEC CWP rises through seawater and a geothermal borehole circulates through soil and/or rock, the governing heat-transfer problem is mathematically identical once lateral seawater advection is neglected: (i) with an internal, forced-convection water stream with mass flow rate $\dot{m}$ and specific heat c_p; (ii) a cylindrical wall with thermal conductivity k_w that provides a purely radial conduction path, and (iii) an external medium, either seawater or saturated ground, at temperature $T_\infty(z)$ that changes slowly with depth. Because Equations (1)–(4) and the Darcy–Weisbach friction factor equation (discussed later) are the same in both applications, with only the parameters being different (such as radius, etc.), matching measured outlet temperatures in geothermal pipes validates the internal-convection, wall-conduction, and solver settings that are also present in the OTEC calculations. Toward this verification process for the CWP, the studies considered were; (i) an OTEC model [78], for verification of the pumping power equations; and (ii) vertical ground heat exchangers [79–82].

Carnot efficiency, which is essentially a theoretical maximum value, can be estimated using only the temperatures of the deep seawater and the surface seawater, using the following equation:

$$\eta_{Carnot} = 1 - \frac{T_{deep\ seawater}}{T_{surface\ seawater}} \tag{5}$$

Another well-known efficiency approximation, using only the temperatures of the heat source and sink, is the Chambadal-Novikov [83] (also referred to as Curzon-Ahlborn [84]) efficiency η_{CN} *or* η_{CA}, which can be described as

$$\eta_{CN} \text{ or } \eta_{CA} = 1 - \sqrt{\frac{T_{deep\ seawater}}{T_{surface\ seawater}}} \tag{6}$$

For both efficiencies, the Carnot and the Chambadal-Novikov efficiency, temperature units are in the Kelvin scale [K]. Choosing a steady temperature of 26 °C (301.15K) for the surface seawater and varying the deep seawater temperature, one can estimate the above-mentioned efficiencies, as shown in Fig. 3.

The required pumping power for the CWP is also of crucial importance as, for the usual lengths of the pipe, it could be in the range of 20–30 % of the generated OTEC system power [85]. The required pumping power can be estimated using the following equation [86,87]:

$$\dot{W}_{p,CWP} = \frac{m_{CWP}\Delta H_{CWP,T} g}{\eta_{p,CWP}} \tag{7}$$

where m_{CWP} is the mass flowrate [kg s^{-1}], $g = 9.81$ m s^{-2} the gravitational acceleration, $\eta_{p,CWP}$ is the pump efficiency assumed at 85 % (or 0.85), and $\Delta H_{CWP,T}$ the total dynamic head difference of the CWP [m] as defined in Refs. [88,89] (see Equation (8)), and $\eta_{p,CWP}$ is the pump hydraulic efficiency. Multiplying m_{CWP} *and* $\Delta H_{CWP,T}$ converts the required head into mechanical power, which is then divided by $\eta_{p,CWP}$ to account for pump losses.

$$\Delta H_{CWP,T} = \Delta H_{CWP,PH} + \Delta H_{CWP,d} + \Delta H_{C,HE} \tag{8}$$

The total head comprises (i) the pipe-related head $\Delta H_{CWP,PH}$ (Equation (9)) caused by friction and fittings, (ii) the hydrostatic or buoyancy head $\Delta H_{CWP,d}$ arising from the density difference between cold and warm seawater columns, and (iii) the additional head $\Delta H_{C,HE}$ required on the condenser side when applicable.

$$\Delta H_{CWP,PH} = \Delta H_{CWP,f} + \Delta H_{CWP,b} \tag{9}$$

$\Delta H_{CWP,f}$ is the head loss due to friction, described by the Darcy-Weisbach, as

$$\Delta H_{CWP,f} = f_D \frac{L_{CWP}}{D_{CWP,i}} \frac{u_{cWP}^2}{2g} \tag{10}$$

where L_{CWP} is the CWP length [m], $D_{CWP,i}$ the inner diameter of the CWP [m], f_D the Darcy–Weisbach dimensionless friction factor, which captures wall roughness and flow regime. The head loss scales linearly with pipe length L_{CWP}, inversely with diameter $D_{CWP,i}$, and quadratically with the mean velocity u_{CWP}, reflecting the kinetic-energy dissipation of the developing turbulent boundary layer. The Colebrook explicit approximation [90] was used for the estimation of f_D, based on the Reynolds number (Re) [91]. On laminar flows with low Re, the Stokes approximation is used and the condition in this case is $f_D = \begin{cases} \frac{64}{Re}, Re < 1000 \\ max\left(f_{Turb}, \frac{64}{Re}\right), Re \geq 1000 \end{cases}$, where $f_{Turb} = \left[1.8 \log\left(\frac{6.9}{Re}\right)\right]^2$. In most scenarios estimated, Re is over 1000, and therefore the f_{Turb} is mostly used. Also, u_{CWP} is the fluid velocity in the CWP [m s^{-1}] expressed as:

$$u_{CWP} = \frac{m_{CWP}}{A_{CWP}\rho_{CWP}} = \frac{m_{CWP} \times 4}{\rho_{CWP} \times \pi \times d_{CWP}^2} \tag{11}$$

where, A_{CWP} is the cross-sectional area of the CWP, and ρ_{CWP} is the cold seawater density. The term $\Delta H_{CWP,b}$ (in equation (9)), defined below, describes the minor losses of the CWP (due to fittings/bends, valves, etc.), which are equivalent to added length to the straight pipe friction losses.

$$\Delta H_{CWP,b} = \frac{u_{CWP}^2}{2g} \sum f_m \tag{12}$$

Here $\sum f_m$ is the sum of minor-loss coefficients for bends, valves and inlets; where each coefficient translates the local disturbance into an 'equivalent length' of straight pipe, which is why the term is of the familiar $\frac{u_{CWP}^2}{2g}$ form. The value of 60 for the sum, as found in the literature [63,92], is applied here. The head difference in regards to the change in density (in equation (8)) is defined as [89].

$$\Delta H_{CWP,d} = L_{CWP} - \frac{1}{\rho_{cs}}\left(\frac{L_{CWP}}{2}\right)(\rho_{ws} + \rho_{cs}) \tag{13}$$

$\Delta H_{CWP,d}$ represents the hydrostatic head generated by the average density difference between the cold seawater (ρ_{ws}, [kg m^{-3}]) and the warmer seawater (ρ_{cs}, [kg m^{-3}]); hence it grows linearly with pipe length L_{CWP}. The head difference due to the condenser is depended on the sizing (capacity of the system) and has an important role on the required power from the pump. However, since in any case of the CWP the condenser will remain the same, it can be neglected in the calculations here. For future reference however, the head difference for the condenser can be defined as

$$\Delta H_{C,HE} = f_C \frac{u_C^2}{2g} \frac{L_C}{(D_{eq})_C} \tag{14}$$

where L_C is the length for the condenser [m], u_C the seawater velocity in the condenser [m s^{-1}], and f_C the friction factor of the condenser, Plate Heat Exchanger (PHE) or Shell and tube, although other choices could be selected, with no real effect on the result despite any possible clogging due to salinity [93,94]), and can be obtained with the Taborek estimation [95]. $(D_{eq})_C$ is the equivalent (hydraulic) diameter (in this case for a noncircular cross section), which can be defined for a PHE as [96]

$$D_{eq} = \frac{4A_{PHE}}{P} \tag{15}$$

where A_{PHE} is the area of the PHE flow [m^2], and P the wetted perimeter [m] (i.e., the short and long sides of the PHE). Other studies [97–100] estimate the $(D_{eq})_C$ as two times the clearance between the plates; this is the case for circular pipes.

Following the methodology and the verification of the model set-up, the results were obtained by the COMSOL Multiphysics 6.1 software. OTEC systems have conventionally a continuous operation and therefore do not require a specific start-up time, or set-up time; however, for the estimation of this model, the initial temperatures were set for non-working conditions, and the model was initially fixed for a time step with one month ending. The time stepping was estimated based on the Backward Differentiation Formula (BDF) with 5 and 1 maximum and minimum BDF order respectively, with the steps taken by the solver set for intermediate stepping; BDF takes at least one step in each subinterval of the times specified.

3. Results and discussion

Firstly, an investigation was conducted on the different approach of between using a realistic geometry of the CWP, and by using a simplified approach. The computation results have indicated that during high flow rates, of 500 kg s^{-1} (or velocities of 1 m s^{-1}) or

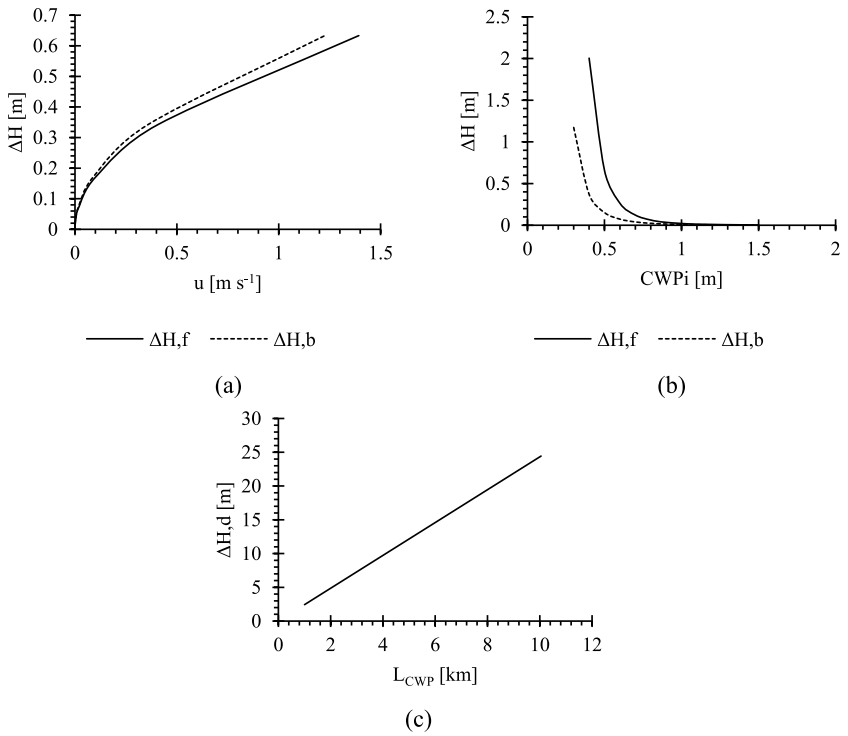

Fig. 4. CWP Head difference: (a) due to friction (ΔH,f) and due to minor/bending losses (ΔH,b), at different fluid velocities, for $D_{CWP,i} = 1.9022$m; (b) at different CWP inner pipe diameters; and (c) due to density difference between the cold deep seawater and the warmer seawater at condenser, at different CWP lengths, for constant mass flowrate of 45 kg s^{-1}.

higher, minimum to no difference (2.1 % or lower) in the output CWP temperature is observed. This can be justified due to the only 20m difference (or less than 1 % difference) in the CWP length. For the smaller flow rates, of 45 kg s^{-1} (or ~0.05 m^3 s^{-1}) or smaller, there is a percentage difference observed at 16.8 % or higher in terms of ΔT between the initial temperature.

Before analyzing the effect of CWP size on ΔT, the head difference through the heat losses along the CWP are investigated. For a fixed mass flowrate of 45 kg s^{-1}, Fig. 4(a) shows the fluid velocity in the CWP (for fixed CWP inner diameter of 1.9022m), Fig. 4(b) the CWP inner diameter with respect to head difference (ΔH), while Fig. 4(c) shows the effect of CWP length with respect to head difference. The total head difference, as explained in Section 2, accounts for the friction losses (equation (10)), minor/bending losses (equation (12)), losses due to the density difference (equation (13)). It must be noted that the greater difference is due to the density difference, which is proportional to the CWP length. The head losses due to friction and minor/bending losses account only for a small percent, <5 % each or <10 % combined, of the total head loss for the CWP, which are also proportional to the velocity and the CWP inner diameter.

For initial results the model set-up was initiated with the temperature at the condenser for one month of continuous operation, for a CWP length of 10 km, as shown in Fig. 5(a) (initial temperature equal to the constant sea surface temperature of the evaporator at 27.3 °C). It can be observed that after one week of operation the temperature reaches a steady state, thus providing the condenser a steady temperature input of 8.7 °C. Note that as the temperature of the deep seawater is at 4.5 °C (marked as a dotted line), yielding an initial ΔT of 22.8 °C, there is a noticeable reduction of 22.7 % in ΔT (between the condenser and the evaporator). A further examination of the temperature along the CWP is presented in Fig. 5(b), where a rapid increase in temperature can be observed for distances of <4 km lengths; this consequently can have a negative effect on the efficiency of the system.

The effect of the mass flowrate and the CWP inner diameter were considered in the study, to determine how these parameters affect the ΔT and consequently the efficiency of the OTEC system. As observed in Fig. 6, using equation (2) for cold seawater density of 1028 kg m^{-3}, sizing down (i.e., reducing the diameter $D_{CWP,i}$) the CWP inner diameter (for fixed mass flowrate of 100 kg s^{-1}) has an insignificant effect (of 3–4 %) on the condenser inlet temperature; however, reducing $D_{CWP,i}$ the pump does require higher pressure and higher pumping power (as seen in Fig. 7, using equation (7)). Based on the requirements of the heat exchanger (sizing depends on the exchange rate required), the cold-water pump is sized accordingly, and since the reduction of $D_{CWP,i}$ does not have a significant effect on ΔT, and consequently nor on the efficiency of the system, $D_{CWP,i}$ should be scaled up in order to reduce the required pumping power. It should also be noted that higher-diameter pipes come at a higher cost, with additional labour installation costs.

On the other hand, as expected, with the reduction of the mass flowrate at the CWP, the temperature difference increases in the range of 96 % (Fig. 6), consequently reducing the OTEC performance by 29 % and 10 % (see equations (5) and (6)) for the 10 km and 5 km respectively. Another major effect observed is the distance from shore/length of CWP to the required deep-sea temperature. It is also clear that temperature difference increases with CWP length, as demonstrated by the two curves of Fig. 6, where an up to 39 % reduction is observed between a 10 km and a 5 km long CWP. However, this variable is mainly controlled by the chosen location, and therefore cannot usually be adjusted at any given location.

The distance from shore (horizontal distance) and hence the length of CWP, required to achieve the desired ΔT, has an effect on the net efficiency of the system, as there is a need for a higher pumping power (see 7(b), using equation (7)), as opposed to the essentially no effect of the diameter of the CWP (see the curves in Fig. 7(a) for five different mass flowrates, where the effect is non-significant above a certain CWP diameter depending on the case). It can be observed that, for fixed inner diameter $D_{CWP,i} = 0.7608$ (from Table 2), the pumping power increases with length by up to 88 %, regardless of mass flowrate. To satisfy the system requirements and to achieve a lower temperature difference between the CWP inlet and the condenser inlet, the mass flowrate is increased (see the curves in Fig. 7 (b) for four different mass flowrates). However, increasing the flowrate increases the required pumping power in a linear manner. For example, increasing the mass flowrate from 45 to 300 kg s^{-1} (~0.045–0.3 m^3 s^{-1}) makes the power to increase by nearly 7 times. Consequently, the effect of increasing the mass flowrate on longer CWPs is a lot stronger than on shorter CWPs in absolute numbers (see curves for powers at 1 km and 10 km). Hence, one can realize the advantage of a floating structure (of CWP length of 1 km) over onshore structures (with CWP lengths of > 2 km) in this respect. This can also be supported in the literature, where case evidence

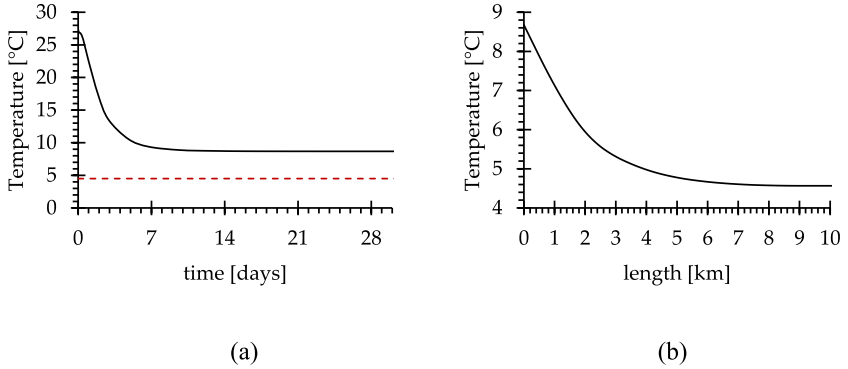

Fig. 5. (a) CWP Temperature versus time at the input of the condenser, with a length of CWP at 10 km and with initial conditions specified in Fig. 1; (b) Temperature variation across along the CWP, with length at points 0 and 10 showing the condenser inlet temperature and seabed temperature at 1 km depth respectively.

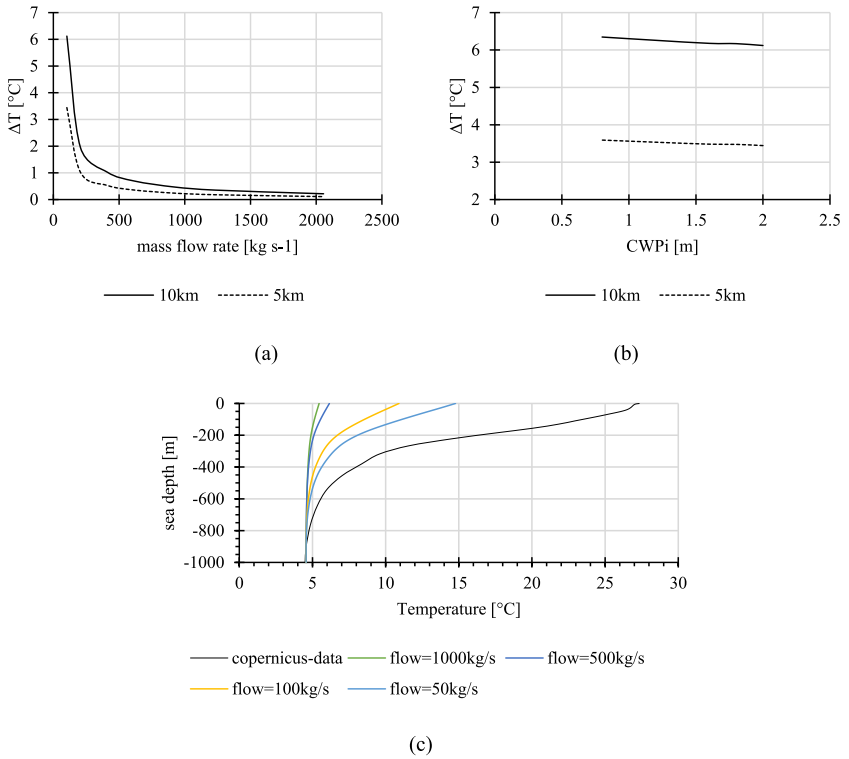

Fig. 6. (a) Mass flowrate, (b) CWP inner diameter, effect on the temperature difference between the condenser inlet and the CWP deep seawater inlet, for two different CWP lengths, 10 km and 5 km. with cold seawater density at 1028 kg m^{-3}; (c) sea depth effect on temperature for a 10 km-long CWP at various mass flowrates.

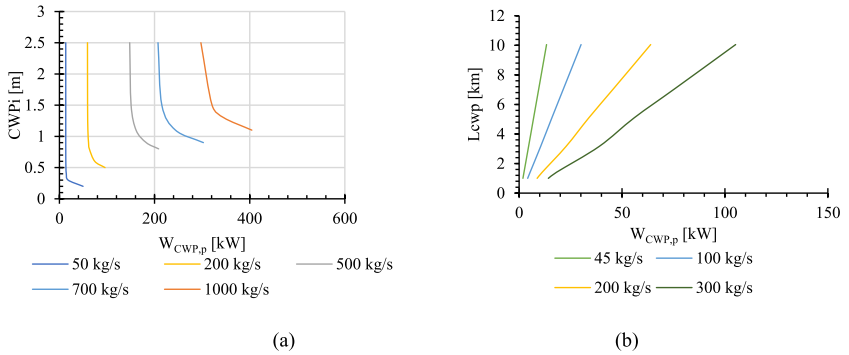

Fig. 7. Cold deep seawater pumping power versus (left-axis) CWP inner diameters for a 10 km-long CWP and (b) CWP pumping power, versus CWP length, for different mass flowrates (m_{CWP}), both with an assumed 85 % pump efficiency.

shows that simply downsizing the pipe to maintain high velocities is rarely economical due to higher pressure drop, offsetting the savings in material and installation [101].

Pumping power requirements are directly affected by the head differences previously reported. The relevant estimated slopes are

Table 3
Projected slope for the Head difference due to friction with different varying paraments.

Head difference	Affected parameter	Slope
ΔH	L_P	20.553
	u_{CWP}	14.698
	$D_{P,i}$	6.854
	f_D	5.394

presented in Table 3. Linear relations for each parameter may be obtained by altering the friction factor, the pipe's length, the fluid's velocity, and the inner diameter of the pipe. Table 3 shows that the greatest slope, and thus the greatest variation in pumping power, is due to the length of the CWP. It is important to remember that the sum is used for the overall pumping power rather than the specific numbers shown in Fig. 3. Lower values of slopes show less of an influence from changes in pumping power caused by the friction factor and inner CWP pipe diameter. Increasing the CWP flow rate, minimizes the time available for heat exchange inside the pipe, resulting in the cold deep seawater "arriving" at the condenser closer to its deep-sea temperature. This cooling benefit dominates even though higher velocities also raise the convective heat-transfer coefficient, which on its own would favor a slightly warmer outlet. Therefore, a larger flow rate accelerates thermal stabilization of the pipe and enhances the thermodynamic efficiency of the OTEC cycle. From a techno-economic perspective, however, the gain is strengthened by the steep rise in hydraulic head and pumping power that accompanies both greater velocity and smaller pipe diameters. This very result was also reported in a cost-optimization study [102]. Consequently, flow-rate decisions should be made within an integrated framework that balances pipe heat-transfer performance, structural constraints and life-cycle economics, as supported in recent multi-objective optimizations [103].

It should also be noted that the presence of biofouling is not expected to cause high changes in pumping power, even if it will influence the friction factor and pipe diameter. In theory, this will overestimate the heat exchanger's performance; nevertheless, when fouling accumulates over time, it will be reduced until the cleaning threshold is reached. The fouling factor can be represented as an additional pipe wall resistance (thermal).

The mass flowrate (left y-axis) as well as the length of the CWP (right y-axis) against the temperature difference between the condenser inlet and the CWP deep seawater inlet, for a fixed $D_{CWP,i} = 0.7608$m (from Table 2) and cold seawater density at 1028 kg m^{-3}, are presented in Fig. 8 (upon using equation (2)). The pumping power, as also reported in Fig. 6, increases with the flowrate, and one would suggest that lower flowrates would be more beneficial. However, the flowrate is a value that depends on the heat exchange rate required and is predefined by the system designer. It can be observed that for all four different CWP lengths considered, namely 10 km, 7 km, 5 km and 3 km, the temperature difference decreases with flowrate. In particular, low temperature differences of <1 °C (which account for low heat losses along the CWP), desired for high efficiency, are observed for high-enough flowrates, which might be hard to achieve for the diameter size chosen. The right y-axis of Fig. 8 presents the case with a mass flowrate of 45 kg s^{-1}, where it can be observed that very high temperature differences (>10 °C) (which account for high heat losses along the CWP) can be obtained. This is a drawback for the selection of an onshore construction of an OTEC system for power production, as the desired ΔT of ~20 °C cannot be attained. Hence, in such cases an offshore floating structure is recommended. Also, for the mass flowrate of 45 kg s^{-1}, the temperature differences between a 10 km and a 7 km, a 5 km, and a 3 km CWP, for an onshore OTEC system, are reduced by 22 %, 39 % and 59 % respectively. Note that (not shown here), for a mass flowrate values of 1050 kg s^{-1} the aforementioned values are 29 %, 48 % and 68 % respectively. Finally, comparing the 10 km with the 1 km CWP length case, which may correspond to an offshore system, the temperature difference reduction is at 86 %. This once more points to a great advantage for the offshore systems providing a higher performance when low flowrates and a long distance from shore is required. Further inspection of Figs. 7(b) and 8, reveals that moving from the floating baseline (1 km vertical riser) to a 10 km shore-tethered pipe reduces the ΔT by ~8.7 °C, while at the same time increasing the required power by a factor of 10. Due to the hydraulic head loss's high dependence on overall length (seen also in Fig. 4), and the heat dissipation's primary dependence on the in-water segment, the distance from shore becomes a dominant factor when flow rates are low or when the total pipe length is closer to the distance from shore (low slopes). Where permitting or environmental constraints could prohibit piling, a moored barge placed offshore could give a comparable thermodynamic benefit.

An assessment of the effect of different pipe materials, namely the HDPE and the FRP, with very similar thermal conductivity values at 0.51 and 0.58 W m^{-1} K^{-1} respectively, is performed. Despite having a slightly higher thermal conductivity (which is not desired in the application under consideration), the FRP pipe requires a higher thickness (in order to effectively resist wave-induced bending), thus providing higher R-values (thermal insulance) than HDPE, with respective values of 0.36 and 0.24 m^2 K W^{-1} for the 4m and 2.4m inner diameter pipes (see Table 2). Regarding the temperature difference between the condenser inlet and the CWP deep seawater inlet, for fixed fluid velocity ($u_{CWP} = 0.1$ m s^{-1}), it turns out that the FRP pipe provides a lower value (0.7 °C) than the one yielding from the HDPE pipe (1.7 °C); this is the case at the highest chosen distance from shore (10 km), using equation (2). At shorter distances, lower differences are estimated. The FRP pipe although having a small advantage over the conventional HDPE pipe on the heat transfer effect, it requires higher costs as it is not mass manufactured. It must be noted though that for higher than 2.4m pipe diameters, HDPE pipes are not available and therefore the use of FRP pipes is essential. For vertical risers on a spar buoy, HDPE could be favored (due to lower weight and lower price) and for diagonal on-shore systems exposed to bending, the use of FRP could be justified.

The investigated CWP in the present study exhibit an increase in the system intake (at the condenser) temperature (depending on the case) of 1.4–8.7 °C. Mao et al. [104] employed a finite-volume model to show a comparable heat gain, but attributed most of the loss to wall conductivity and insulation thickness rather than the distance from shore; they recommended thicker insulation or alternative materials once the pipe exceeds several hundred meters. Another finite-volume analysis by Firmansyah et al. [105] on a 5 km onshore pipe found a more modest 1–3 °C rise and likewise stressed the need to account for in-pipe warming when sizing onshore OTEC plants. These current findings therefore align well with the literature results where the results suggest that for long, near-isothermal risers on floating platforms, material and insulation choices dominate, whereas for onshore configurations the horizontal distance itself becomes the principal driver of thermal degradation. On the other hand, hydraulic parameters follow a similar hierarchy. In the current study, pumping power grows by up to 88 % as the CWP lengthens from 1 km to 10 km (depending on the flowrate case), while increasing the inner diameter beyond 0.8 m has minimum influence on ΔT, yet reduces head loss. Mao et al. [104] likewise reported that larger diameters benefit the hydraulics, whereas outlet temperature is much more sensitive to insulation thickness and flow rate.

Finally, with the potential climate changing, an increase of 1 °C in the seawater surface temperature, could decrease ΔT by <5 %

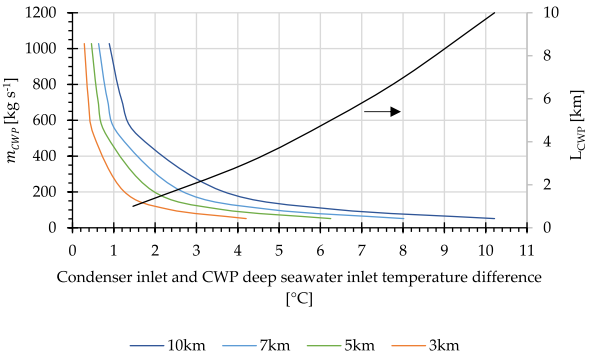

Fig. 8. Temperature difference between the condenser inlet and the CWP deep seawater inlet for different mass flowrates (left y-axis) and CWP lengths with mass flowrate of 45 kg s^{-1} (right y-axis) (for fixed $D_{CWP,i}$ = 0.7608m and cold seawater density = 1028 kg m^{-3}).

due to the "warmer" layer pipe exposure. This surface temperature increase however will have a benefit on the thermodynamic cycle, as it potentially provides a higher performance and output. Another comment, not examined in this study, is that the rejected heat is essentially a high-quality low-grade heat (23–26 °C) that can be harvested for seawater air-conditioning, aquaculture, pre-heating of desalination feed, or even as an input to a 5th generation district heating and cooling networks. Integrating such by-products can recover power otherwise lost.

4. Conclusions

This study has presented a computational investigation of the heat transfer losses through the flow of cold seawater from the deep sea to the sea surface along a cold-water pipe (CWP). The methodology has been described in detail in Section 2. COMSOL Multiphysics software has been used as the main computational tool for the analysis, based on a series of relevant equations gathered from the literature. Due to the lack of experimental data, a verification was performed based on cases in the literature for OTEC and equivalent geothermal energy systems. The main results indicate the following.

The inner diameter of the pipe is not of significant importance in terms of the temperature difference between the cold seawater intake of the CWP and the inlet to the condenser, with only a 3–4 % change for mass flowrate of 100 kg s^{-1}, regardless of CWP length.

The (horizontal) distance from shore is a factor, mostly not human-depended but location-depended, for onshore OTEC systems to reach the required temperature and depths (approximately 1 km). This distance determines the length of the CWP and is of crucial importance, as an extended length of 10 km provides values of ΔT that are not beneficial towards a viable OTEC system. Onshore systems with different CWP lengths, namely 7 km, 5 km, and 3 km, exhibit a temperature difference reduction of 22 %, 39 % and 59 %, compared to a 10 km long CWP, respectively. Offshore CWP and systems (with a CWP of 1 km) exhibit an even lower temperature difference, estimated at up to 86 % from that of the 10 km long CWP. Regarding the mass flowrate effect on temperature difference, the latter decreases with flowrate in the range of 96 % for a 10 km long CWP. The flowrates, however, assume values that the system designer would have to consider in terms of the exchange rate in the condenser, and therefore cannot be varied dramatically.

The relation between the required pumping power and the size (diameter and length) of the CWP has also been investigated. First, as expected, the pumping power increases with mass flowrate for fixed CWP size. Then, the diameter does not seem to significantly affect the pumping power, while the length seems to play a significant role as the pumping power may increase with length by up to 88 %, regardless of mass flowrate.

Comparing HDPE and FRP pipes can show that FRP despite having slightly higher thermal conductivity, due to its larger wall thickness offers higher R-values. FRP exhibits lower temperature differences over high CWP lengths, but comes with higher costs. However, the use of FRP is necessary for large-diameter applications where HDPE pipes are unavailable.

Finally, the overall results indicate that, considering the non-ideal case of heat loss along the CWP, OTEC systems maintain their potential for a viable installation. However, the depth of the sea and the horizontal distance from shore (i.e., the CWP length) remain the most crucial factors. It can be particularly noted, that if the required distance from shore is in the range of 10 km or greater, the possibility of the offshore floating structure should be considered. Floating structures, although at higher cost and risk, would provide a higher efficiency in such cases. It is expected that the return of investment and the payback period could be potentially higher than onshore systems, but this remains to examined and verified through a cost and probably an environmental assessment.

CRediT authorship contribution statement

Lazaros Aresti: Writing – original draft, Software, Methodology, Conceptualization. **Toula Onoufriou:** Writing – review & editing, Supervision, Project administration, Funding acquisition. **Constantine Michailides:** Writing – review & editing, Supervision. **Paul Christodoulides:** Writing – review & editing, Supervision, Conceptualization.

Data availability statement

Not applicable.

Funding

This research was funded by CETPartnership, the European Partnership under Joint Call 2022 for research proposals, co-funded by the European Commission (GA N°101069750) and with the funding organisations listed on the CETPartnership website; see Research and Innovation Foundation of Cyprus under Grant agreement EP/CETP/0922/0055.

Declaration of competing interest

The authors declare that they have no known competing financial interests or personal relationships that could have appeared to influence the work reported in this paper.

Acknowledgments

The authors gratefully acknowledge the Ministry of Energy, Commerce, and Industry of Cyprus and the Cyprus University of Technology.

Data availability

No data was used for the research described in the article.

References

[1] H. Uehara, The present status and future of ocean thermal energy conversion, Int. J. Sol. Energy 16 (1995) 217–231, https://doi.org/10.1080/01425919508914278.
[2] L. Meegahapola, L. Udawatta, S. Witharana, The ocean thermal energy conversion strategies and analysis of current challenges, in: ICIIS 2007 - 2nd International Conference on Industrial and Information Systems 2007, Conference Proceedings, 2007, pp. 123–128, https://doi.org/10.1109/ICIINFS.2007.4579160.
[3] H. Yuan, N. Mei, P. Zhou, Performance analysis of an absorption power cycle for ocean thermal energy conversion, Energy Convers. Manag. 87 (2014) 199–207, https://doi.org/10.1016/J.ENCONMAN.2014.07.015.
[4] Y. Ikegami, T. Yasunaga, T. Morisaki, Ocean thermal energy conversion using double-stage rankine cycle, J. Mar. Sci. Eng. 6 (2018) 21, https://doi.org/10.3390/jmse6010021.
[5] W. Liu, X. Xu, F. Chen, Y. Liu, S. Li, L. Liu, Y. Chen, A review of research on the closed thermodynamic cycles of ocean thermal energy conversion, Renew. Sustain. Energy Rev. 119 (2020) 109581, https://doi.org/10.1016/J.RSER.2019.109581.
[6] I.M. Hernández-Romero, F. Nápoles-Rivera, A. Flores-Tlacuahuac, L.F. Fuentes-Cortés, Optimal design of the ocean thermal energy conversion systems involving weather and energy demand variations, Chem. Eng. Process. Process Intensif. 157 (2020) 108114, https://doi.org/10.1016/J.CEP.2020.108114.
[7] M. Wang, R. Jing, H. Zhang, C. Meng, N. Li, Y. Zhao, An innovative Organic Rankine Cycle (ORC) based Ocean Thermal Energy Conversion (OTEC) system with performance simulation and multi-objective optimization, Appl. Therm. Eng. 145 (2018) 743–754, https://doi.org/10.1016/J.APPLTHERMALENG.2018.09.075.
[8] E.N. Ganic, L. Moeller, Performance study of an OTEC system, Appl. Energy 6 (1980) 289–299, https://doi.org/10.1016/0306-2619(80)90019-7.
[9] Y. Zhang, J. Deng, Z. Deng, Thermodynamic and economic analysis of ocean thermal energy conversion system using zeotropic mixtures, Case Stud. Therm. Eng. 64 (2024), https://doi.org/10.1016/j.csite.2024.105408.
[10] Z. Zhang, H. Yuan, S. Yi, Y. Sun, W. Peng, N. Mei, Theoretical analysis on temperature-lifting cycle for ocean thermal energy conversion, Energy Convers. Manag. 300 (2024) 117946, https://doi.org/10.1016/J.ENCONMAN.2023.117946.
[11] K. Fontaine, T. Yasunaga, Y. Ikegami, OTEC maximum net power output using carnot cycle and application to simplify heat exchanger selection, Entropy 21 (2019), https://doi.org/10.3390/e21121143.
[12] T.H. Soukissian, D. Denaxa, F. Karathanasi, A. Prospathopoulos, K. Sarantakos, A. Iona, K. Georgantas, S. Mavrakos, Marine renewable energy in the Mediterranean Sea: status and perspectives, Energies 10 (2017) 1–56, https://doi.org/10.3390/en10101512.
[13] H. Kobayashi, S. Jitsuhara, H. Uehara, The Present Status and Features of OTEC and Recent Aspects of Thermal Energy Conversion Technologies, 1995.
[14] A.F. Charwat, S.L. Ridgway, The mist-lift OTEC cycle, Energy 5 (1980) 511–524, https://doi.org/10.1016/0360-5442(80)90075-4.
[15] L.A. Vega, Ocean Thermal Energy Conversion, 1995. Enclopedia, New York, NY.
[16] E.N. Ganic, L. Moeller, Performance study of an OTEC system, Appl. Energy 6 (1980) 289–299, https://doi.org/10.1016/0306-2619(80)90019-7.
[17] H. Uehara, The present status and future of ocean thermal energy conversion, Int. J. Sol. Energy 16 (1995) 217–231, https://doi.org/10.1080/01425919508914278.
[18] H. Kobayashi, S. Jitsuhara, H. Uehara, The Present Status and Features of OTEC and Recent Aspects of Thermal Energy Conversion Technologies, 1995.
[19] L. Aresti, P. Christodoulides, C. Michailides, T. Onoufriou, Reviewing the energy, environment, and economy prospects of Ocean Thermal Energy Conversion (OTEC) systems, Sustain. Energy Technol. Assessments 60 (2023) 103459, https://doi.org/10.1016/j.seta.2023.103459.
[20] Y. Rami, A. Allouhi, 3E (Energy, Exergy and Economic) multi-objective optimization of a novel solar-assisted ocean thermal energy conversion system for integrated electricity and cooling production, Energy Convers. Manag. 321 (2024), https://doi.org/10.1016/j.enconman.2024.119006.
[21] J. Hurtt, A. Pellen, J. Nagurny, OTEC power efficiency challenges, Proceed. Annual Offshore Technol. Conf. 1 (2010) 732–743, https://doi.org/10.4043/20498-ms.
[22] S.E. Rizea, Optimization of Ocean Thermal Energy Conversion Power Plants, Electronic Theses and Dissertations, 2012, p. 78.
[23] M. Faizal, M.R. Ahmed, Experimental studies on a closed cycle demonstration OTEC plant working on small temperature difference, Renew. Energy 51 (2013) 234–240, https://doi.org/10.1016/J.RENENE.2012.09.041.
[24] K. Rajagopalan, G.C. Nihous, Estimates of global Ocean Thermal Energy Conversion (OTEC) resources using an ocean general circulation model, Renew. Energy 50 (2013) 532–540, https://doi.org/10.1016/J.RENENE.2012.07.014.
[25] D. Walraven, B. Laenen, W. D'Haeseleer, Comparison of thermodynamic cycles for power production from low-temperature geothermal heat sources, Energy Convers. Manag. 66 (2013) 220–233, https://doi.org/10.1016/j.enconman.2012.10.003.

[26] M. Ascari, H. Hanson, L. Rauchenstein, J. Van Zwieten, D. Bharathan, D. Heimiller, N. Langle, G.N. Scott, J. Potemra, E. Jansen, N.J. Nagurny, Ocean Thermal Extractable Energy Visualization, 2012.
[27] C. Bernardoni, M. Binotti, A. Giostri, Techno-economic analysis of closed OTEC cycles for power generation, Renew. Energy 132 (2019) 1018–1033, https://doi.org/10.1016/J.RENENE.2018.08.007.
[28] T. Yasunaga, K. Fontaine, Y. Ikegami, Performance evaluation concept for ocean thermal energy conversion toward standardization and intelligent design, Energies 14 (2021) 1–12, https://doi.org/10.3390/en14082336.
[29] A. Etemadi, A. Emdadi, O. AsefAfshar, Y. Emami, Electricity generation by the Ocean thermal energy, Energy Proc. 12 (2011) 936–943, https://doi.org/10.1016/J.EGYPRO.2011.10.123.
[30] W. Liu, X. Xu, F. Chen, Y. Liu, S. Li, L. Liu, Y. Chen, A review of research on the closed thermodynamic cycles of ocean thermal energy conversion, Renew. Sustain. Energy Rev. 119 (2020) 109581, https://doi.org/10.1016/J.RSER.2019.109581.
[31] R. Magesh, OTEC technology- A world of clean energy and water, WCE 2010 - World Congr. Eng. 2 (2010) 1618–1623, 2010.
[32] J.H. VanZwieten, L.T. Rauchenstein, L. Lee, An assessment of Florida's ocean thermal energy conversion (OTEC) resource, Renew. Sustain. Energy Rev. 75 (2017) 683–691, https://doi.org/10.1016/J.RSER.2016.11.043.
[33] J. Koto, R.B. Negara, Study on ocean thermal energy conversion in Morotai Island, North Maluku, Indonesia, J. Aeronaut. Sci. Eng. 7 (2016) 7.
[34] M.G. Petterson, H. Ju Kim, Can ocean thermal energy conversion and seawater utilisation assist small island developing states? A case study of Kiribati, Pacific Islands Region, Ocean Thermal Energy Conv. (OTEC) Past Present Progress (2020) 1–28, https://doi.org/10.5772/intechopen.91945.
[35] R. Adiputra, T. Utsunomiya, J. Koto, T. Yasunaga, Y. Ikegami, Preliminary design of a 100 MW-net ocean thermal energy conversion (OTEC) power plant study case: mentawai island, Indonesia, J. Mar. Sci. Technol. 25 (2020) 48–68, https://doi.org/10.1007/s00773-019-00630-7.
[36] A. García Huante, Y. Rodríguez Cueto, R. Silva, E. Mendoza, L. Vega, Determination of the potential thermal gradient for the Mexican Pacific Ocean, J. Mar. Sci. Eng. 6 (2018) 20, https://doi.org/10.3390/jmse6010020.
[37] T. Yasunaga, Y. Ikegami, Finite-time thermodynamic model for evaluating heat engines in ocean thermal energy conversion, Entropy 22 (2020) 211, https://doi.org/10.3390/e22020211.
[38] Y. Ikegami, T. Yasunaga, T. Morisaki, Ocean thermal energy conversion using double-stage rankine cycle, J. Mar. Sci. Eng. 6 (2018), https://doi.org/10.3390/jmse6010021.
[39] Y. Ikegami, T. Morisaki, OTEC using multi-stage rankine cycle, in: Proceedings of the Twenty-Third (2013) International Offshore and Polar Engineering, International Society of Offshore and Polar Engineers (ISOPE), Anchorage, Alaska, USA, 2013 880653.
[40] W. Liu, X. Xu, F. Chen, Y. Liu, S. Li, L. Liu, Y. Chen, A review of research on the closed thermodynamic cycles of ocean thermal energy conversion, Renew. Sustain. Energy Rev. 119 (2020) 109581, https://doi.org/10.1016/J.RSER.2019.109581.
[41] M. Wang, R. Jing, H. Zhang, C. Meng, N. Li, Y. Zhao, An innovative Organic Rankine Cycle (ORC) based Ocean Thermal Energy Conversion (OTEC) system with performance simulation and multi-objective optimization, Appl. Therm. Eng. 145 (2018) 743–754, https://doi.org/10.1016/J.APPLTHERMALENG.2018.09.075.
[42] K. Rajagopalan, G.C. Nihous, Estimates of global Ocean Thermal Energy Conversion (OTEC) resources using an ocean general circulation model, Renew. Energy 50 (2013) 532–540, https://doi.org/10.1016/j.renene.2012.07.014.
[43] A. Giostri, A. Romei, M. Binotti, Off-design performance of closed OTEC cycles for power generation, Renew. Energy 170 (2021) 1353–1366, https://doi.org/10.1016/j.renene.2021.02.047.
[44] Y. Zhou, Z. xiang Zheng, G. si Zhao, Analytical models for heat transfer around a single ground heat exchanger in the presence of both horizontal and vertical groundwater flow considering a convective boundary condition, Energy 245 (2022) 123159, https://doi.org/10.1016/J.ENERGY.2022.123159.
[45] R. Saeidi, Y. Noorollahi, V. Esfahanian, Numerical simulation of a novel spiral type ground heat exchanger for enhancing heat transfer performance of geothermal heat pump, Energy Convers. Manag. 168 (2018) 296–307, https://doi.org/10.1016/J.ENCONMAN.2018.05.015.
[46] M. Meikandan, M. Sundarraj, D. Yogaraj, K. Malarmohan, Experimental and numerical investigation on bare tube cross flow heat exchanger-using COMSOL, Int. J. Ambient Energy 41 (2020) 500–510, https://doi.org/10.1080/01430750.2018.1472650.
[47] W. Engels, F. Zabihian, Principle and preliminary calculation of Ocean thermal energy conversion, principle and preliminary calculation of ocean thermal, Energy Convers. (2014) 1–5.
[48] H. Aydin, Performance Analysis of a Closed- Cycle Ocean Thermal Energy Conversion System with Solar, 2013, p. 82.
[49] J.I. Yoon, S.H. Seol, C.H. Son, S.H. Jung, Y.B. Kim, H.S. Lee, H.J. Kim, J.H. Moon, Analysis of the high-efficiency EP-OTEC cycle using R152a, Renew. Energy 105 (2017) 366–373, https://doi.org/10.1016/J.RENENE.2016.12.019.
[50] J. Hurtt, A. Pellen, J. Nagurny, OTEC power efficiency challenges, Proceed. Annual Offshore Technol. Conf. 1 (2010) 732–743, https://doi.org/10.4043/20498-ms.
[51] Y. Du, H. Peng, J. Xu, Z. Tian, Y. Zhang, X. Han, Y. Shen, Performance analysis of ocean thermal energy conversion system integrated with waste heat recovery from offshore oil and gas platform, Case Stud. Therm. Eng. 54 (2024) 104027, https://doi.org/10.1016/J.CSITE.2024.104027.
[52] H.J. Kim, H.S. Lee, S.T. Lim, M. Petterson, The suitability of the Pacific islands for harnessing ocean thermal energy and the feasibility of OTEC plants for onshore or offshore processing, Geosciences 11 (2021), https://doi.org/10.3390/geosciences11100407.
[53] P. Kapranos, R. Priestner, Overview of metallic materials for heat exchangers for ocean thermal energy conversion systems, J. Mater. Sci. 22 (1987) 1141–1149, https://doi.org/10.1007/BF01233102.
[54] C. Bernardoni, M. Binotti, A. Giostri, Techno-economic analysis of closed OTEC cycles for power generation, Renew. Energy 132 (2019) 1018–1033, https://doi.org/10.1016/J.RENENE.2018.08.007.
[55] K. Keesmaat, Installation of a Large Diameter Cold Water Pipe in Deepwater for a Land-based OTEC Plant, Tudelft, 2015.
[56] Lockheed Martin, NAVFAC Ocean Thermal Energy Conversion (OTEC) Project, Manassas, Virginia, USA, 2010.
[57] B. Cable, W. Tayler, C. Tindal, R. Varley, L. Brissey, The Navy's Ocean Thermal Energy Conversion Program, MTS/IEEE Seattle, OCEANS 2010, 2010, https://doi.org/10.1109/OCEANS.2010.5664608.
[58] Lockheed Martin, NAVFAC Ocean Thermal Energy Conversion (OTEC) Project, Manassas, Virginia, USA, 2010.
[59] T.E. Little, Ocean Thermal Energy Conversion Program, Maryland, Annapolis, 1978.
[60] W. Griekspoor, Ocean thermal energy conversion, Resour. Conserv. 7 (1981) 49–60, https://doi.org/10.1016/0166-3097(81)90019-5.
[61] A. Giostri, A. Romei, M. Binotti, Off-design performance of closed OTEC cycles for power generation, Renew. Energy 170 (2021) 1353–1366, https://doi.org/10.1016/j.renene.2021.02.047.
[62] M.G. Petterson, H. Ju Kim, Can ocean thermal energy conversion and seawater utilisation assist small island developing states? A case study of Kiribati, Pacific Islands Region, Ocean Thermal Energy Conv. (OTEC) Past Present Progress (2020) 1–28, https://doi.org/10.5772/intechopen.91945.
[63] A. Giostri, A. Romei, M. Binotti, Off-design performance of closed OTEC cycles for power generation, Renew. Energy 170 (2021) 1353–1366, https://doi.org/10.1016/j.renene.2021.02.047.
[64] U. Berardi, N. Dembsey, Thermal and fire characteristics of FRP composites for architectural applications, Polymers 7 (2015) 2276–2289, https://doi.org/10.3390/polym7111513.
[65] H.B. Survey, V. Levu, Reducing Vulnerability of Pacific ACP States FIJI TECHNICAL REPORT October 2008, 2008. October.
[66] P. Christodoulides, A. Vieira, S. Lenart, J. Maranha, G. Vidmar, R. Popov, A. Georgiev, L. Aresti, G. Florides, Reviewing the modeling aspects and practices of shallow geothermal energy systems, Energies 13 (2020) 4273, https://doi.org/10.3390/en13164273.
[67] I.I. Stylianou, S. Tassou, P. Christodoulides, L. Aresti, G. Florides, Modeling of vertical ground heat exchangers in the presence of groundwater flow and underground temperature gradient, Energy Build. 192 (2019) 15–30, https://doi.org/10.1016/j.enbuild.2019.03.020.
[68] L. Aresti, G.A. Florides, P. Christodoulides, Computational modelling of a ground heat exchanger with groundwater flow, Bulg. Chem. Commun. 48 (2016) 55–63.

[69] L. Aresti, P. Christodoulides, G.P. Panayiotou, G. Florides, Residential buildings' foundations as a ground heat exchanger and comparison among different types in a moderate climate country, Energies 13 (2020) 6287, https://doi.org/10.3390/en13236287.
[70] M.H. Sharqawy, New correlations for seawater and pure water thermal conductivity at different temperatures and salinities, Desalination 313 (2013) 97–104, https://doi.org/10.1016/j.desal.2012.12.010.
[71] N.P. Fofonoff, R.C. Millard Jr., Algorithms for computation of fundamental properties of seawater, UNESCO Tech. Pap. Mar. Sci. 44 (1983) 1–53.
[72] G.S.K. Wong, S. ming Zhu, Speed of sound in seawater as a function of salinity, temperature, and pressure, J. Acoust. Soc. Am. 97 (1995) 1732–1736, https://doi.org/10.1121/1.413048.
[73] C.T. Chen, F.J. Millero, Speed of sound in seawater at high pressures, J. Acoust. Soc. Am. 62 (1977) 1129–1135, https://doi.org/10.1121/1.381646.
[74] IOC, SCOR, IAPSO, The international thermodynamic equation of seawater-2010: calculation and use of thermodynamic properties, in: Intergovernmental Oceanographic Commission, Manuals and Guides No.56, UNESCO, 2010.
[75] T.J. McDougall, P.M. Barker, Getting Started with TEOS-10 and the Gibbs Seawater (GSW) Oceanographic Toolbox, SCOR/IAPSO WG127, 2011.
[76] X. Yang, Y. Liu, Y. Chen, L. Zhang, Optimization design of the organic rankine cycle for an ocean thermal energy conversion system, Energies 15 (2022), https://doi.org/10.3390/en15186683.
[77] T. Yasunaga, T. Noguchi, T. Morisaki, Y. Ikegami, Basic heat exchanger performance evaluation method on OTEC, J. Mar. Sci. Eng. 6 (2018), https://doi.org/10.3390/jmse6020032.
[78] X. Yang, Y. Liu, Y. Chen, L. Zhang, Optimization design of the organic rankine cycle for an ocean thermal energy conversion system, Energies 15 (2022), https://doi.org/10.3390/en15186683.
[79] I.I. Stylianou, P. Christodoulides, L. Aresti, S. Tassou, G. Florides, Borehole ground heat exchangers and the flow of underground water, International Journal of Industrial Electronics and Electrical Engineering (2018) 67–72.
[80] I.I. Stylianou, S. Tassou, P. Christodoulides, L. Aresti, G. Florides, Modeling of vertical ground heat exchangers in the presence of groundwater flow and underground temperature gradient, Energy Build. 192 (2019) 15–30, https://doi.org/10.1016/j.enbuild.2019.03.020.
[81] L. Aresti, G.A. Florides, P. Christodoulides, Computational modelling of a ground heat exchanger with groundwater flow, Bulg. Chem. Commun. 48 (2016) 55–63.
[82] P. Christodoulides, A. Vieira, S. Lenart, J. Maranha, G. Vidmar, R. Popov, A. Georgiev, L. Aresti, G. Florides, Reviewing the modeling aspects and practices of shallow geothermal energy systems, Energies 13 (2020) 4273, https://doi.org/10.3390/en13164273.
[83] A. Vaudrey, F. Lanzetta, M. Feidt, H.B. Reitlinger, The origins of the efficiency at maximum power formula for heat engines, J. Non-Equilibrium Thermodyn. 39 (2014) 199–203, https://doi.org/10.1515/jnet-2014-0018.
[84] F.L. Curzon, B. Ahlborn, Efficiency of a carnot engine at maximum power output, Am. J. Phys. 43 (1975) 22–24, https://doi.org/10.1119/1.10023.
[85] L. Meegahapola, L. Udawatta, S. Witharana, The ocean thermal energy conversion strategies and analysis of current challenges, in: ICIIS 2007 - 2nd International Conference on Industrial and Information Systems 2007, Conference Proceedings, 2007, pp. 123–128, https://doi.org/10.1109/ICIINFS.2007.4579160.
[86] W. Zhang, Y. Li, X. Wu, S. Guo, Review of the applied mechanical problems in ocean thermal energy conversion, Renew. Sustain. Energy Rev. 93 (2018) 231–244, https://doi.org/10.1016/j.rser.2018.05.048.
[87] R.H. Yeh, T.Z. Su, M.S. Yang, Maximum output of an OTEC power plant, Ocean Eng. 32 (2005) 685–700, https://doi.org/10.1016/J.OCEANENG.2004.08.011.
[88] M.A.T. Chik, S. Sarip, Y. Ikegami, M.Y. Amyra, N. Othman, R. Yacob, H. Hara, Z. Zakaria, H. Izzuan, Design optimization of power generation and desalination application in Malaysia utilizing ocean thermal energy, J. Teknol. 77 (2015) 177–185.
[89] H. Uehara, Y. Ikegami, Optimization of a closed-cycle OTEC system, J. Sol. Energy Eng. 112 (1990) 247–256, https://doi.org/10.1115/1.2929931.
[90] C.F. Colebrook, Turbulant flow in pipes, with particulat reference to the transition region between the smooth and rough pipe laws, J. Inst. Civil Eng. 11 (1939) 133–156, https://doi.org/10.1680/ijoti.1939.13150.
[91] D. Brkić, Review of explicit approximations to the Colebrook relation for flow friction, J. Pet. Sci. Eng. 77 (2011) 34–48, https://doi.org/10.1016/j.petrol.2011.02.006.
[92] M.Z. Malik, F. Musharavati, S. Khanmohammadi, M.M. Baseri, P. Ahmadi, D.D. Nguyen, Ocean thermal energy conversion (OTEC) system boosted with solar energy and TEG based on exergy and exergo-environment analysis and multi-objective optimization, Sol. Energy 208 (2020) 559–572, https://doi.org/10.1016/j.solener.2020.07.049.
[93] M.P. Eldred, J.C. Van Ryzin, S. Rizea, I.C. Chen, R. Loudon, N.J. Nagurny, S. Maurer, E. Jansen, A. Plumb, M.R. Eller, V.R.R. Brown, Heat Exchanger Development for Ocean Thermal Energy Conversion, OCEANS'11 - MTS/IEEE Kona, 2011, https://doi.org/10.23919/oceans.2011.6107175. Program Book.
[94] F. Chen, L. Liu, J. Peng, Y. Ge, H. Wu, W. Liu, Theoretical and experimental research on the thermal performance of ocean thermal energy conversion system using the rankine cycle mode, Energy 183 (2019) 497–503, https://doi.org/10.1016/j.energy.2019.04.008.
[95] E.U. Schltinder, K.J. Bell, D. Chisholm, G.F. Hewitt, F.W. Schmidt, D.B. Spalding, J. Tahorek, A. Zukauskas, V. Gnielinski, Heat Exchanger Design Handbook, Hemisphere Publishing Corporation, 1983.
[96] E.U. Schltinder, K.J. Bell, D. Chisholm, G.F. Hewitt, F.W. Schmidt, D.B. Spalding, J. Tahorek, A. Zukauskas, V. Gnielinski, Heat Exchanger Design Handbook, Hemisphere Publishing Corporation, 1983.
[97] N.A.H.B.M. Yusoff, Optimization of solar assisted ocean thermal energy conversion plant design and system performance, Universiti Teknologi Malaysia (2020).
[98] P. Ahmadi, I. Dincer, M.A. Rosen, Performance assessment of a novel solar and ocean thermal energy conversion based multigeneration system for coastal areas, Journal of Solar Energy Engineering, Transactions of the ASME 137 (2015), https://doi.org/10.1115/1.4028241.
[99] M.A.T. Chik, S. Sarip, Y. Ikegami, M.Y. Amyra, N. Othman, R. Yacob, H. Hara, Z. Zakaria, H. Izzuan, Design optimization of power generation and desalination application in Malaysia utilizing ocean thermal energy, J. Teknol. 77 (2015) 177–185.
[100] M.Z. Malik, F. Musharavati, S. Khanmohammadi, M.M. Baseri, P. Ahmadi, D.D. Nguyen, Ocean thermal energy conversion (OTEC) system boosted with solar energy and TEG based on exergy and exergo-environment analysis and multi-objective optimization, Sol. Energy 208 (2020) 559–572, https://doi.org/10.1016/j.solener.2020.07.049.
[101] R.D. Fuller, Ocean thermal energy conversion, Ocean Manag. 4 (1978) 241–258, https://doi.org/10.1016/0302-184X(78)90026-4.
[102] J. Langer, C. Infante Ferreira, J. Quist, Is bigger always better? Designing economically feasible ocean thermal energy conversion systems using spatiotemporal resource data, Appl. Energy 309 (2022) 118414, https://doi.org/10.1016/J.APENERGY.2021.118414.
[103] L. Mao, C. Wei, S. Zeng, M. Cai, Heat transfer mechanism of cold-water pipe in ocean thermal energy conversion system, Energy 269 (2023) 126857, https://doi.org/10.1016/J.ENERGY.2023.126857.
[104] A.I. Firmansyah, Mukhtasor, D. Satrio, S. Rahmawati, H. Ikhwani, W.A. Pratikto, A study of the temperature distribution in the OTEC cold water pipe using a heat and mass transfer approach, in: IOP Conf Ser Earth Environ Sci, Institute of Physics, 2024, https://doi.org/10.1088/1755-1315/1372/1/012018.